Improvement of *meta*-tetra(Hydroxyphenyl)chlorin-Like Photosensitizer Selectivity with Folate-Based Targeted Delivery. Synthesis and in Vivo Delivery Studies

Julien Gravier,[†] Raphaël Schneider,[‡,*] Céline Frochot,[‡] Thierry Bastogne,[§] Frédéric Schmitt,[⊥] Jacques Didelon,[||] François Guillemin,[§] and Muriel Barberi-Heyob[§]

SRSMC, Structure et Réactivité des Systèmes Moléculaires Complexes, Nancy University, BP 239, F-54506 Vandoeuvre-lès-Nancy, France, DCPR, Département de Chimie Physique de Réactions, Nancy University, CNRS, 1 rue Grandville, BP 20451, F-54001 Nancy, France, CRAN, Centre de Recherche en Automatique de Nancy, Nancy University, CNRS, CAV, Avenue de Bourgogne, F-54511 Vandoeuvre-lès-Nancy, CAV, Centre Alexis Vautrin, Nancy University, University Institute of Pathology, CHUV, Bugnon 25, CH-1011 Lausanne, Switzerland

Received February 6, 2008

The cell membrane folate receptor (FR) is a molecular target for tumor-selective drug delivery, including delivery of photosensitizers for anticancer photodynamic therapy (PDT). Tumor selectivity of *meta*-tetra(hydroxyphenyl)chlorin (*m*-THPC), a photosensitizer used in PDT clinical trials, demonstrates a low tumor-to-normal epithelial uptake ratio. We report on the synthesis and on the photophysical properties of a *m*-THPC-like photosensitizer **1** conjugated to folic acid (compound **8**). A comparative study of the accumulation of photosensitizers **1** and **8** is described. Nude mice were xenografted with FR-α-positive KB or HT-29 cells lacking FR-α as a negative control. Using optical fiber fluorimetry, we demonstrated that conjugate **8** exhibited enhanced accumulation in KB tumors compared to **1** 4 h after injection. No significant difference between KB and HT-29 tumors was observed in case of compound **1**. Tumor-to-normal tissue ratio exhibited a very interesting selectivity for conjugate **8** (5:1) in KB tumors 4 h postinjection.

Introduction

Photodynamic therapy (PDT)[a] is one of the noninvasive ways of treating malignant tumors or macular degeneration.[1,2] In the photodynamic reaction, the photosensitizer, or photosensitizing agent, promoted to the excited singlet state using light, decays to the triplet state and generates highly reactive oxygen species (ROS) such as singlet oxygen through intermolecular triplet−triplet energy transfer to oxygen. The ROS produced are toxic to cells and tissues and destroy cancer cells.[3–5]

The essential element in the development of PDT is the photosensitizer that absorbs light of an appropriate wavelength at the site of photodynamic reaction to produce ROS and gives the desired therapeutic outcome. Over the past decade, a substantial effort has been put into the development of various classes of photosensitizers that present better absorption, greater tumor specificity, and less cutaneous photosensitivity compared to the first-generation photosensitizer Photofrin (a mixture of hematoporphyrin Hp oligomers currently used in PDT treatment).[6–8] Compared to porphyrins, chlorins offer increased absorption in the farthest-red side band, thus enabling the use of a light with deeper penetration in organic tissues. Moreover, chlorins present good singlet oxygen quantum yields, making them overall better photosensitizers and attractive for use in PDT. Among chlorins, *meta*-tetrahydroxyphenylchlorin (*m*-THPC, temoporfin, Foscan) is a second-generation photosensitizer clinically used for the treatment of human mesothelioma and for gynecological, respiratory, and head and neck cancers.[9] Despite its high photodynamic efficacy, *m*-THPC, like most of the current photosensitizing agents, has a relatively narrow therapeutic window and is associated with significant side effects such as photosensitivity upon exposure to sunlight due to skin accumulation.[10,11] Moreover, many misleading informations concerning the distribution of this photosensitizer in tissues can be found in the literature. For example, Westerman et al. reported on a selectivity around 3−4 at 2−8 h after administration of *m*-THPC in nude mice with a human colon carcinoma model (LS174T).[12] In contrast to these results, no selectivity has been observed between human mesothelioma xenograft and muscle in nude BALB/c mice for similar short times after administration of *m*-THPC[13] or only a little selectivity within a mammary carcinoma model in C3D2/F1 mice.[14]

Recently, several new strategies have emerged to improve the performances of PDT agents, including conjugation with oligonucleotides, monoclonal antibodies, epidermal growth factor, carrier proteins, carbohydrates, or hydrophilic polymers for selective delivery of the agents into tumor tissues.[9,15–17] However, the lack of specific targets of chlorin- and porphyrin-based photosensitizers and the dark cytotoxicity still remain a major challenge for PDT. The vitamin folic acid is a ligand able to target covalently attached bioactive agents quite specifically to folate receptor (FR)-positive cancer cells.[18,19] The FR, which is a well-known cancer cell-associated protein, can actively internalize bound folates via endocytosis.[20,21] Folate receptors exist in three major forms, namely FR-α, FR-β, and FR-γ. The FR-α form is overexpressed by many types of tumor cells, including ovarian, endometrial, colorectal, breast, lung, renal, neuroendocrine carcinomas, and brain metastases.[18,22] Upon receptor interaction, the folic acid−receptor complex is taken up by cells and moves into many organelles involved in endocytotic trafficking, providing for cytosolic deposition.[23] Proper synthesis procedures have been pointed out to link folic acid to molecules in order to develop targeting delivery systems. It was demonstrated

* To whom correspondence should be addressed. Phone: + 33 3 83 68 21 56. Fax: + 33 3 83 68 21 54. E-mail: raphael.schneider@pharma.uhp-nancy.fr.

[†] SRSMC, Nancy University.

[‡] DCPR, Nancy University.

[§] CRAN, Nancy University.

[||] CAV, Nancy University.

[⊥] Pathology Institute, Lausanne University.

[a] Abbreviations: Boc, *tert*-butoxycarbonyl; DCC, dicyclohexylcarbodiimide; EDC, 1-[3-(dimethylamino)propyl]-3-ethylcarbodiimide hydrochloride; FR, folate receptor; NMP, *N*-methylpyrrolidinone; PDT, photodynamic therapy; PEG, poly(ethylene glycol); Φ_F: fluorescence quantum yield; $\Phi(^1O_2)$: singlet oxygen quantum yield; ROS, reactive oxygen species; *m*-THPC, *meta*-tetrahydroxyphenylchlorin; THF, tetrahydrofuran.

10.1021/jm800125a CCC: $40.75
Published on Web 06/14/2008

Scheme 1. Synthesis Route to tris(3-Hydroxyphenyl)-4-carboxyphenylchlorin

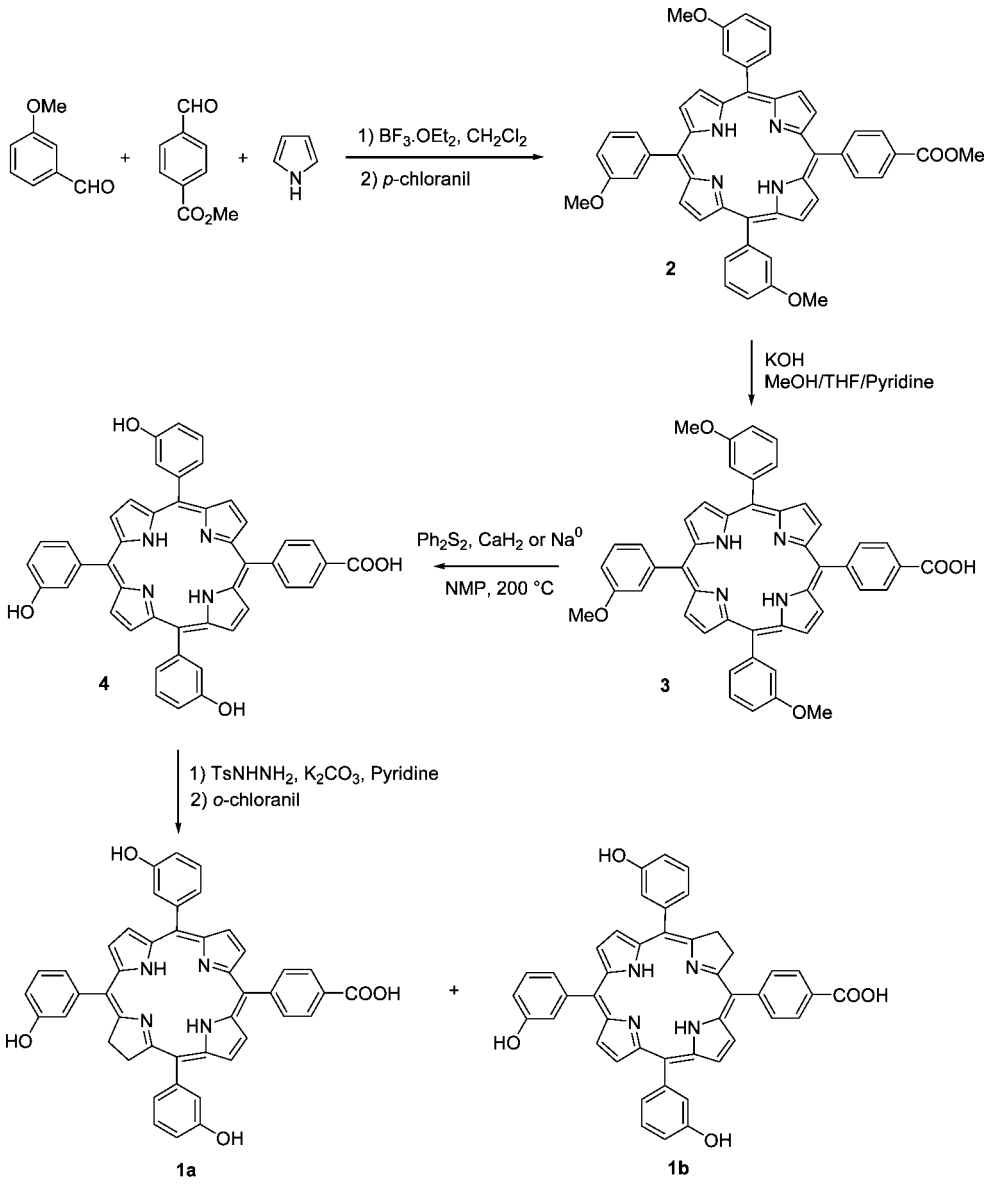

that the glutamate γ-carboxyl group modification does not induce significant loss of folic acid affinity for the receptor.[20] Moreover, because of its high stability, compatibility with both organic and aqueous solvent, low cost, nonimmunogenic character, ability to conjugate with a wide variety of molecules, and low molecular weight, folic acid has attracted wide attention as a targeting agent for tumor detection. Recent examples that take advantage of folic acid uptake to promote targeting and internalization include inorganic nanoparticles,[24,25] polymer nanoparticles,[26,27] polymeric micelles,[28] lipoprotein nanoparticles,[29] tumor imaging agents,[30] cyclodextrins,[31] chemotherapeutics,[32] microgels,[33] and dendrimers[34] (see refs 19, 35, and 36 for a comprehensive overview of this technology).

Our group synthesized a new porphyrin−folic acid conjugate using a short poly(ethylene glycol) (PEG), 2,2′-(ethylenedioxy)-bis-ethylamine, as a spacer arm. Our preliminary in vitro studies, developed with KB nasopharyngeal cells, a human nasopharyngeal epidermal carcinoma cell line overexpressing FR-α form, demonstrated that the uptake of the conjugate was on average 7-fold higher than tetraphenylporphyrin used as a reference and that the cells were significantly more sensitive to folic acid-conjugated porphyrin-mediated PDT.[37] Very recently, Stefflova et al. succeeded in the development of a fluorescent photosensitizer−peptide−folic acid conjugate for PDT and near-infrared fluorescence imaging and demonstrated its good biodistribution pattern (FR-specific tumor uptake and low accumulation in normal tissues).[38] In the present study, we first report on the synthesis and photophysical properties of a *m*-THPC-like photosensitizer conjugated to folic acid via 2,2′-(ethylenedioxy)-bis-ethylamine **8**. We subsequently describe a comparative study of accumulation of compound **8** in KB tumors, used as positive control, and in HT-29 tumors, lacking FR-α as negative control. An optical fiber spectrofluorimeter was used to follow the fluorescence accumulation of the conjugate **8** versus the nonconjugated photosensitizer **1** by fluorescence spectroscopy in real-time in tumor-bearing nude mice.

Results and Discussion

Chemistry. One of the goals of our synthetic work in this area was the successful preparation of a structurally related derivative of *m*-THPC bearing a *para*-carboxylic group for the linkage chemistry. Tris(3-hydroxyphenyl)-4-carboxyphenylchlorin **1** was synthesized according to Scheme 1 starting from 3-methoxybenzaldehyde, methyl 4-formylbenzoate, and pyrrole.

Scheme 2. Synthesis Route to the tris(3-Hydroxyphenyl)-4-carboxyphenylchlorin Conjugated with Folic Acid (Only One Isomer of the Chlorine and the γ-Folate Conjugate is Represented for Simplicity)

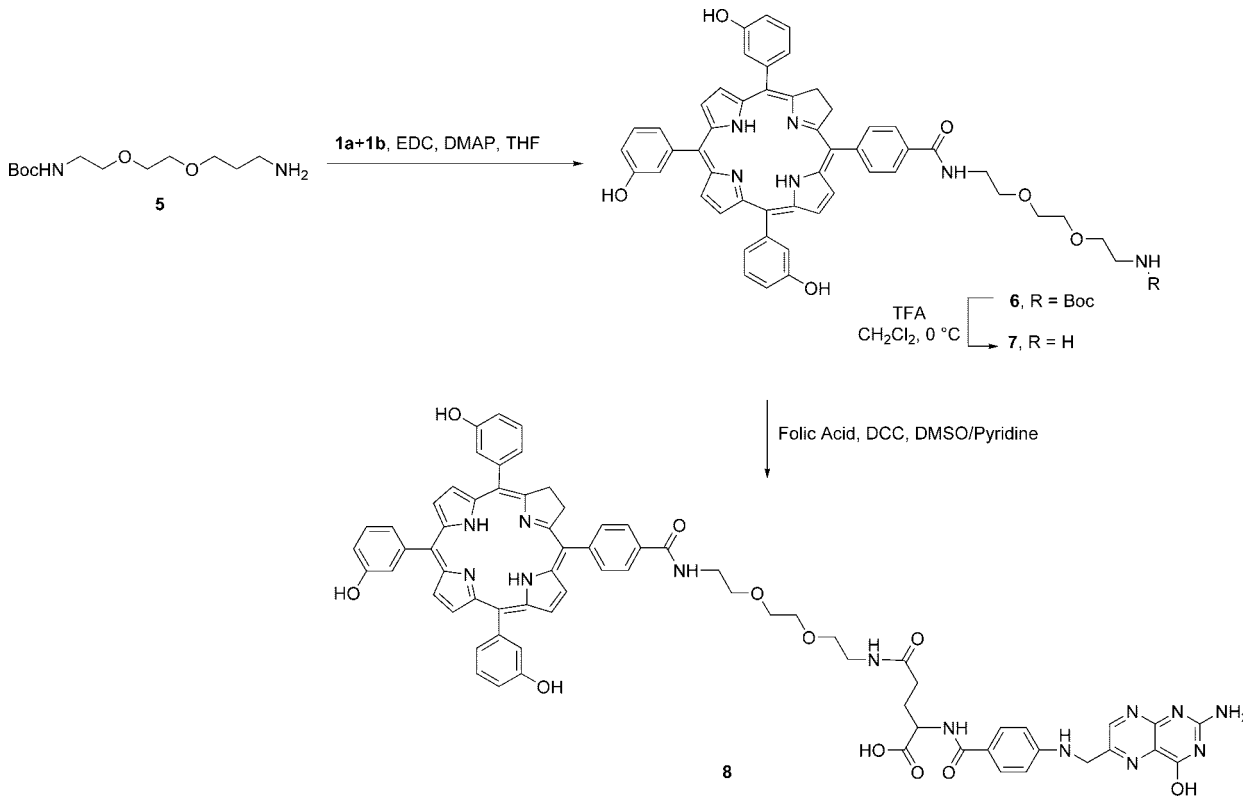

After 2.5 h stirring at room temperature in CH_2Cl_2 in the presence of $BF_3 \cdot OEt_2$, the intermediate porphyrinogen was oxidized in situ with 2,3,5,6-tetrachlorobenzoquinone (*p*-chloranil) in refluxing CH_2Cl_2 to yield porphyrin **2** in 8% yield after column chromatography. The ester function of **2** was subsequently hydrolyzed with KOH to generate the acid **3**. Compound **3** proved to be extremely resistant to classical demethylation methods. Despite varying many reaction parameters such as reaction temperature, solvent, or number of equivalents, no satisfactory results were obtained when demethylation of **3** was attempted with BBr_3 or HBr (partial demethylation and only traces of **4**). Rapid and complete deprotection could however be achieved by treatment of **3** with Ph_2S_2 and sodium metal or CaH_2 in NMP to generate the demethylating thiophenate anion.[39,40] Tris(3-hydroxyphenyl)-4-carboxyphenylporphyrine **4** was isolated as a crystalline solid with an excellent 90% yield after column chromatography using this experimental procedure. Diimide reduction of porphyrin **4** using toluene-4-sulfonohydrazide in dry pyridine afforded chlorin **1** and the corresponding bacteriochlorin, which was carefully reoxidized at 25 °C with *o*-chloranil until the absorption peak at 735 nm disappeared.[41] After column chromatography, the isomeric chlorins **1a** and **1b** (a 50/50 mixture of two inseparable isomers) were obtained in 78% yield. Finally, it should be noted that when the diimide reduction of the porphyrin **3** was performed before the demethylation step, a partial oxidation of tris(3-hydroxyphenyl)-4-carboxyphenylchlorin into the corresponding porphyrin (up to 45%) was observed during the heating with the thiophenate anion.

The synthesis of the target compound **8** was carried out as described in Scheme 2. Chlorins **1** were first linked to Boc-monoprotected 2,2′-(ethylenedioxy)-bis-ethylamine **5** by an EDC-mediated coupling reaction with a 85% yield. Deprotection of the Boc group with TFA followed by DCC-mediated coupling of compound **7** with folic acid afforded the folate-coupled chlorins **8** in 79% yield. For administration to animals, crude **8** was first dialyzed against saline and water to remove unreacted starting materials and byproduct and then purified by RP-HPLC (see Supporting Information).

Because carbodiimide-activated folic acid can be coupled with chlorins **7** via either α- or γ-carboxyl groups of its glutamate residue, and that only the γ-conjugate is capable of binding to the FR,[42] it was important to determine the relative amounts of each α- and γ-carboxyl-linked conjugates. By RP-HPLC and ^{1}H NMR, we determined that ca. 70% of the chlorins **7** were linked through the γ-carboxyl group. These proportions of α- and γ-products are consistent with the previously reported results obtained during coupling of folic acid with amine derivatives.[43] Only the γ-folate conjugate of isomeric chlorins, isolated in 51% yield from crude **8** by RP-HPLC, was used for in vivo experiments.

Spectroscopic Characterization and Photophysical Properties. The absorption spectra of chlorin **1** and conjugate **8** in ethanol are shown in Figure 1, and optical properties of selected compounds synthesized are gathered in Table 1. The absorption spectra of compound **8** appears additive as it is made of visible bands that can be assigned to the chlorin, namely the intense Soret band at ca. 415 nm and the weaker Q-bands at longer wavelengths and of bands that are attributed to the folic acid unit in the UV region. Interaction of chlorin and folic acid seems negligible as far as the electronic absorption viewpoint is concerned. The fluorescence quantum yields were calculated by steady state comparative method using tetraphenylporphyrin as reference and were comparable for **1**, **8**, and *m*-THPC. It can finally be noted that conjugate **8** showed simultaneously the fluorescence emission corresponding to folic acid at 350 nm (Figure 2) and chlorin typical fluorescence emission specific at 652 nm (Figure 3). Singlet oxygen formation quantum yields

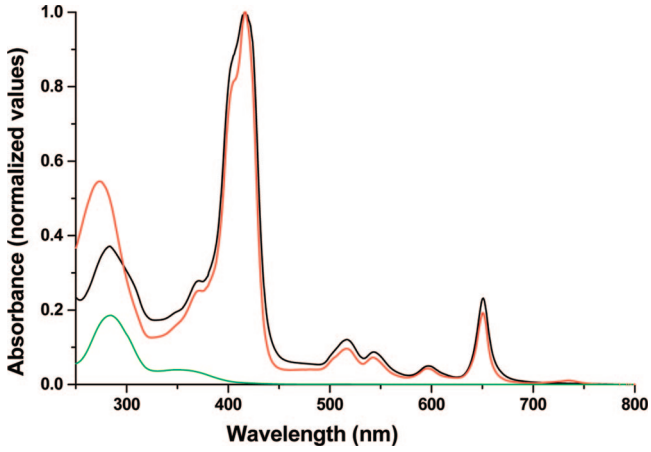

Figure 1. Absorption spectra of folic acid (green line), chlorin **1** (red line), and of conjugate **8** (black line).

were determined by direct measurement of the infrared luminescence (1270 nm) using Bengal pink in ethanol as reference and were similar for compounds **1**, **8**, and *m*-THPC.

Expression of FR-α by KB and HT-29 Cell Lines. To validate the choice of the KB nasopharyngeal cell line, as a positive control overexpressing FR-α (FR^+), and HT-29 cells, a human colon adenocarcinoma cell line, lacking FR-α (FR^-), the expression of FR-α was investigated. KB cells strongly expressed FR-α (Figure 4). Western blot analysis revealed the presence of high levels of FR-α as shown by a strong band at 40 kDa. As previously shown by Parker et al.,[22] no expression of FR-α was observed in HT-29 cells. HeLa cells also expressed RF-α, albeit to a lesser extent than KB cells, suggesting that conjugate **8** could also be used for the selective delivery of photosensitizers to this cell line.

Effect of Tissue Optics on Fluorescence Measurements and Spectral Analysis. As an initial animal model, we employed the athymic mouse implanted subcutaneously with KB cells, which overexpress the FR-α, but it is expected that the results obtained with this tumor model can be extended to other human tumors known to overexpress FR-α.[44,45] Experiments were performed with an optical fiber spectrofluorimeter built in our laboratory. Bourdon et al. have demonstrated that in situ fluorescence measurements with fiber fluorimetry and concentration data determined by HPLC after extraction were in broad agreement, indicating that this noninvasive technique is sufficiently sensitive and can be used to follow the distribution of fluorescent drugs in real time.[46]

Tumor-bearing nude mice were intravenously injected with 2.2×10^{-6} mol/kg of compounds **8** or **1**. For fluorescence measurements, the distal end of the probe was placed in gentle contact with the tissue area to be investigated (skin or tumor). Three or two animals, depending on problems with intravenous injection or tumor development, were tested for each condition and averaged, representing intertissue variations for one animal.

The light absorption and scattering properties of tissues may have an important influence on both the intensity and spectral shape of measured fluorescence. With short-wavelength excitation (blue, λ ca. 410 nm), the high light attenuation by tissue restricts measurements to superficial layers and makes them sensitive to local tissue inhomogeneities because hemoglobin and other natural chromophores like flavins have high absorption. Thus, fluorescence spectra were first normalized to the flavins fluorescence mean intensity.[47] In fact, autofluorescence in the red region of the visible spectrum typically consists of two components. The first one is a monotonically decreasing "tail" composed of emission from a number of endogenous fluorophores with emission maxima at shorter wavelengths, and the second component is emission from naturally occurring porphyrins in the tissue. Because the proportions of these two components may vary with time and among animals, it was necessary to treat them as separate basis spectra. An algorithm based on a Bayesian approach coupled to a Markov chain Monte Carlo method was used (for spectral analysis, see Experimental Section). Figure 5 shows representative fluorescence spectra estimated by this spectral analysis and illustrates the effect of tissue optics on fluorescence measurements corresponding to compound **8** accumulation in tumor and skin 4 and 24 h postinjection. We measured the highest fluorescence signals in the tumors and the weakest coming from the skin. Moreover, spectral distribution and peak intensities were found to be reproducible whatever the animal used for the same experimental conditions (see Supporting Information for all spectra).

The Role of Folate Attachment for Selective Delivery of Conjugate 8. To create a suitable animal model for evaluation of FR targeting in vivo, athymic mice were implanted subcutaneously with about 10^6 human nasopharyngeal carcinoma (KB) cells, previously used in the study of FR targeting in vitro.[37] Measurable tumors consistently developed 10−15 days after cells implantation. Upon section at the time of study, the tumors had a negligible degree of necrosis (data not shown). Successful execution of this study required an animal model that would mimic human neoplastic disease both in terms of the folate receptor content of the tumor but also of the free-folate concentration in the serum. Because normal rodent chow contains a high concentration of folic acid (6 mg/kg of chow), the mice used in the tumor-targeting studies were maintained on folate-free diet to achieve serum folate concentrations closer to the 4−6 μg/L (9−14 nM) range of normal human serum.[48] Hence, the comparative study of photosensitizer accumulation was performed after 2−3 weeks of folate-free diet. To monitor the tissue uptake by fluorescence of compounds **8** and **1** and to validate the FR-targeting selectivity of the conjugated photosensitizer in vivo, nude mice bearing either a KB tumor (FR^+) or a HT-29 tumor (FR^-) were used after the drugs injection at two different time points (4 and 24 h postinjection). Both photosensitizers accumulation within tumor tissues was higher than in the skin, independently of the FR-α expression tumor status or animal's diet (Figures 5 and 6). Unsurprisingly, we noticed differences in skin fluorescence at 4 h postinjection for both photosensitizers (Figure 6A) and for compound **8** in mice on a folate-free diet (Figure 6 B). Indeed, the limited number of mice for each condition, conceivable interindividual variations in pharmacokinetics (mainly at short-times) associated with very low fluorescence intensities values measured in the skin, and a period varying from 2 to 3 weeks of fed folate-free rodent diet, all emphasize the variability in individual responsiveness and contribute to this apparent difference between animals. Four hours after intravenous injection, conjugate **8** exhibited enhanced in vivo accumulation in KB tumors (around 2.0-fold) compared to **1** but only for the folic acid-free animal's diet. The specific involvement of the FR in mediating this uptake is demonstrated by no **8** accumulation in KB tumor for the mice that were fed normal (high folate) rodent chow (Figures 6A,B). However, 24 h postinjection and for mice under folate-free diet, no further accumulation of **8** in FR^+ tumors was observed (Figure 6D), probably due to a more rapid elimination of **8** from the blood compartment compared to **1**. Indeed, photosensitizers **1** and **8** will have different pharmacokinetics because the delivery mechanism and their hydrophobicity differ. Active transport via

Table 1. Electronic Absorption, Fluorescence Data, and Singlet Oxygen Quantum Yield for **1**, **8**, and *m*-THPC Derivatives[a]

compound	λ_{max} (nm) (ε)[b]	fluorescence λ_{max} (nm)[c]	fluorescence quantum yield [Φ_F]	singlet oxygen quantum yield [$\Phi(^1O_2)$]
1	417(33.3), 517(2.4), 542(1.8), 597(1.0), 650(4.7)	652	0.20	0.72
8	283(11.0), 417(28.0), 517(3.5), 542(2.6), 596(1.5), 650(6.8)	652	0.18	0.57
m-THPC	417(81.0), 517(10.8), 542(6.8), 596(4.3), 650(21.8)	654	0.24	0.60

[a] All UV−vis and fluorescence spectra were recorded in EtOH. [b] Molar extinction coefficients are expressed in 10^3 M^{-1} cm^{-1}. [c] Fluorescence spectra were recorded after excitation at ca. 415 nm.

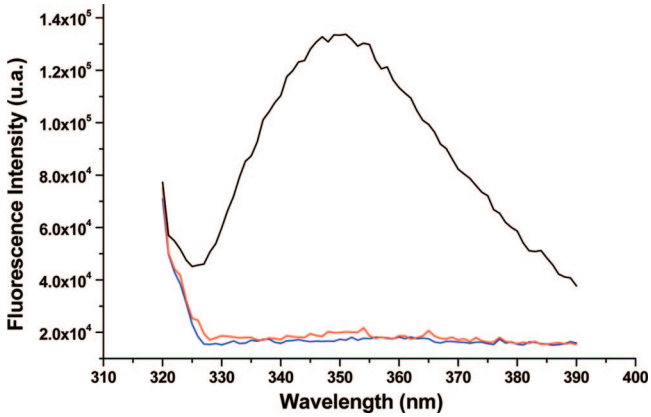

Figure 2. Fluorescence spectra of *m*-THPC (blue line), chlorin **1** (red line), and conjugate **8** (black line) after excitation at λ_{ex} = 290 nm (spectra were corrected relative to absorbance).

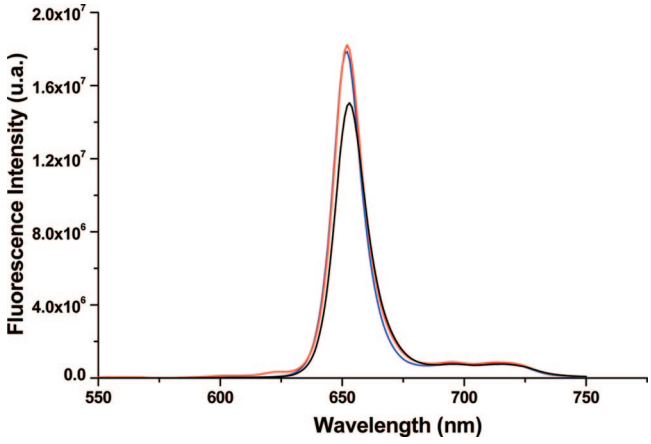

Figure 3. Photoluminescence spectra of *m*-THPC (blue line), chlorin **1** (red line), and conjugate **8** (black line) after excitation at λ_{ex} = 420 nm (spectra were corrected relative to absorbance).

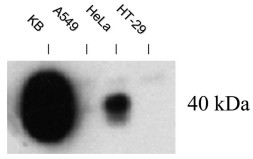

Figure 4. Western blot analysis of FR-α expression by KB, A549, HeLa, and HT-29 cells. A549 cells were added as negative control. KB cells strongly overexpressed FR. HeLa cells also expressed FR-α, albeit to a lesser extent than KB cells.

receptor-mediated endocytosis, where the compound is trapped within an endosome, combined with generally rapid clearance of more hydrophilic compounds from the system, will result in shorter times between the injection and maximum tumor accumulation compared to hydrophobic photosensitizers that can both be taken up by endocytosis but also freely penetrate the membrane and often circulate longer within the system. One additional aspect that is important for folic-acid-mediated drug delivery concerns the rate of FR recycling between the cell surface and its intracellular compartments. Accumulation of folate conjugates in tumors tissues will depend upon not only the number and accessibility of FR on the malignant cell surfaces but also the time required for unoccupied receptors to recycle back to the cell surface for additional drug uptake. Using radioactive conjugates, Paulos et al. found empty FR^+ to unload their cargo and return to the cell surface in about 8−12 h.[49] As previously shown, folate-conjugated radiotracers were found to be efficiently cleared from the blood compartment 24 h postintravenous administration to rats. Hence, as there was no substantial radiotracer accumulation 4 h postinjection, folate-receptor-targeted radiopharmaceuticals were used after that intravenous administration period.[43,49]

A light loss of **8** uptake in FR^- tumor as well as a decrease of its uptake in skin were observed for the animals maintained on folate-free diet compared to those receiving normal dietary sources (Figure 6). A starvation of folic acid in the animal's diet for three weeks unavoidably leads to a decrease in cellular metabolic activity, illustrated by lower values of the photosensitizer accumulation in normal tissue. Folic acid is an essential dietary vitamin used by all eukaryotic cells for DNA synthesis and one-carbon metabolism. It was found that the porphyrin production after intraperitoneal injection of 5-aminolevulinic acid (ALA) or its derivative methyl 5-aminolevulinate (MAL) was significantly increased by intraperitoneal injection of folic acid. Folic acid might be used for the protection of normal skin against photosensitization. The effects of folic acid were demonstrated to be similar in tumors and normal skin.[50]

A factorial ANOVA (analysis of variance) modeling method was used to evaluate which parameter or combination (tumor type, diet, photosensitizer type, postinjection time, or tissue type) leads to the best photosensitizer accumulation. Five two-level biological factors were considered (Table 2). The determination coefficient r^2 for the full factorial model was about 0.84, which is a satisfactory result for an in vivo model. Estimates of the ANOVA model coefficients are listed in Table 3. Biological factors X_3, X_5 and interactions between X_1 and X_2, X_3, and X_4 demonstrated a statistically significant effect ($P > 0.001$) on the photosensitizer accumulation in tissues (Table 3). Photosensitizer type and tissue type lead to the most important impacts on photosensitizer accumulation. The interaction between photosensitizer type and postinjection time was also significant, confirming that simultaneously both factors interact with the response.

Tumor-to-Normal Tissue Ratio as a Result of Selectivity. Each condition was tested at least in two tumor-bearing nude mice. Experimental design was applied to analyze tumor-to-skin accumulation ratio 4 h postinjection, corresponding for conjugate **8** to the optimum accumulation time in the FR^+ tumor. Tables 4 and 5 list the main mean effects on the in vivo selectivity, calculated from the estimated model. Results indicated an interesting selectivity 5.0 versus 2.1 for conjugate **8** compared to **1** in FR-bearing KB tumors for animals under a folic acid-free diet (Tables 4 and 5). This clearly shows the effect of the folate carrier, which facilitates the preferential

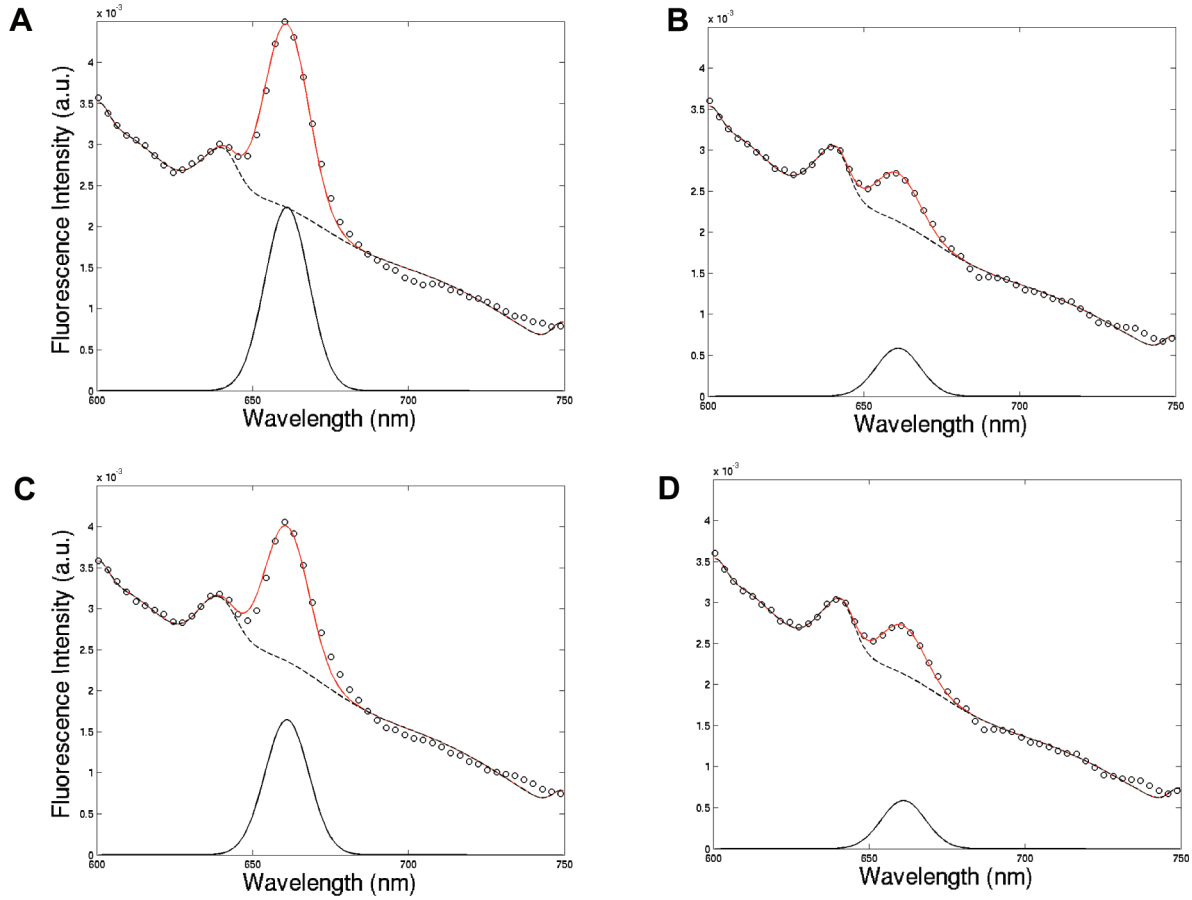

Figure 5. Representative fluorescence emission spectra after excitation at 410 nm in KB tumor tissue recorded from a living mouse 4 h (A) and 24 h (C) after intravenous administration of **8** (2.2×10^{-6} mol/kg). (B,D) Fluorescence emission spectra in normal epithelial tissue (skin) recorded from a mouse for the same conditions. Spectra were normalized relative to the tissue autofluorescence. Each spectrum was a mean fluorescence spectrum calculated from three spectra measured at different points of the tissue. Measured fluorescence spectrum (circle). Estimated fluorescence spectrum obtained by fitting with an algorithm based on a Bayesian approach coupled to a Markov chain Monte Carlo method (red line). Isolated Gaussian function from the estimated model of the complete spectrum (black dotted line) and the estimated photosensitizer-free fluorescence spectrum (black line).

accumulation of **8** in the KB tumor because folate-lacking **1** does not distinguish between the FR^+ and FR^- tumors. Our results are consistent with those obtained by Stefflova et al., who developed a folate derivative of the pyropheophorbide photosensitizer for imaging and PDT. Their compound accumulated more in KB tumors than in HT1080 cells (FR^-) (ca. 2.5 fold).[38] Tumor selectivity of *m*-THPC has also been investigated on animal models in vivo.[51–55] No conclusions have been drawn in as far as drug concentration in specific tissues varied depending on species and individuals.[56] It may be considered that a tumor-to-normal epithelial ratio of 1 to 1.5 has been currently observed using optical fiber fluorimetry on patients undergoing PDT of esophageal tumors with *m*-THPC (J. Blais, personal communication, unpublished data, see ref 46). Using fluorimetric technique, Morlet et al. observed a tumor fluorescence maximum at 72 h postinjection but with a tumor-to-skin ratio decreasing between 12 and 72 h.[52] As expected, when we compare the in vivo selectivity of **8** in mice fed on normal diet, there is no difference between FR^+ KB tumors and FR^- HT-29 tumors (Table 4) because serum folate from normal dietary sources will directly compete with the folate conjugate for tumor cell uptake via the folate receptor pathway. This is consistent with the observation of Mathias et al., who demonstrated that a ^{67}Ga−deferoxamine−folate conjugate, used as a tumor-selective radiopharmaceutical, showed marked tumor-specific deposition in vivo 4 h post injection. In this study, the authors have also noticed that tumor uptake of their conjugate was blocked by intravenous preadministration of free folate as well as by maintaining the animals on normal folate-rich rodent chow.[48]

Conclusion

In conclusion, we have prepared and characterized a new folic acid-conjugated *m*-THPC like photosensitizer **8**. Its tissue accumulation was evaluated in vivo by optical fiber fluorimetry. Results obtained show that 4 h after intravenous injection, folate-specific uptake of conjugate **8** was enhanced in KB tumors (ca. 2.0 fold) compared to the nonconjugated photosensitizer **1**. Moreover, the selectivity for tumor versus normal tissue was high (5:1). The observed behavior of compounds **8** and **1** at 4 h versus 24 h postinjection is likely due to the combination of a specific uptake and a more rapid clearance of **8** from blood. Through a factorial analysis of variance modeling method, we have finally demonstrated that the photosensitizer structure (targeted **8** or nontargeted **1**) and tissue type (KB cell line overexpressing FR or HT-29 cell line lacking FR) are the most important parameters on photosensitizer accumulation. Because the mean free path of singlet oxygen is very short (>0.05 μm), the resultant apoptosis and necrosis occur only in cells that have taken up the photosensitizer. We therefore hope that conjugate **8** can be proposed for improved selectivity in PDT of folate

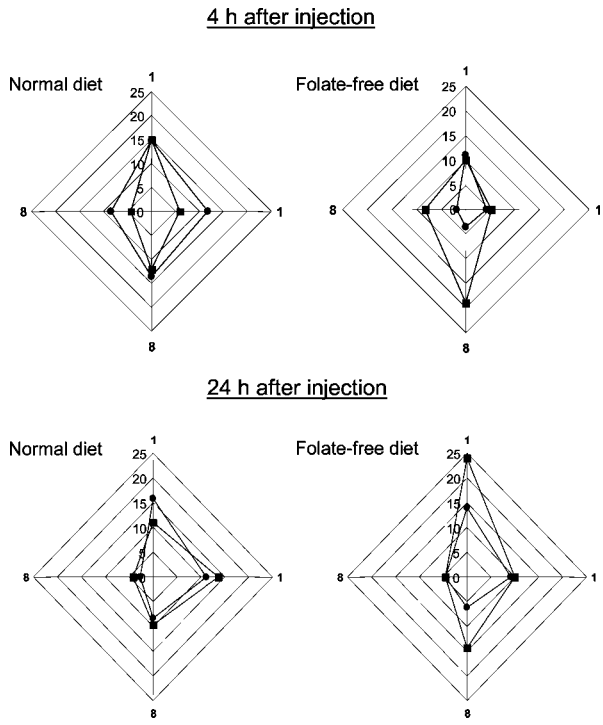

Figure 6. In vivo accumulation of photosensitizers (Z values $\times 10^{-4}$, see Spectral Analysis in Experimental Section) in KB (square) or HT-29 (circle) tumors (Y-axis) and in skin (X-axis). Data were obtained after intravenous injection of **8** or **1** ($2.2.10^{-6}$ mol/kg).

Table 2. Biological Factors of the Full Factorial Experiment

symbol	definition	levels	coded values	factors
X_1	tumor cells type	2	−1/1	KB cells/HT-29 cells
X_2	diet	2	−1/1	without folate/with folate
X_3	photosensitizer type	2	−1/1	**8/1**
X_4	postinjection time	2	−1/1	4 h/24 h
X_5	tissue type	2	−1/1	tumor/skin

Table 3. Estimates of the Model Coefficients and their Significance

coefficient	estimate	F value Pr (>F)	coefficient	estimate	F value Pr (>F)
Y_0	1.77×10^{-6}	*d*	b_{123}	-1.98×10^{-7}	*d*
b_1	-3.17×10^{-7}	*b*	b_{124}	4.22×10^{-8}	*d*
b_2	2.02×10^{-7}	*a*	b_{125}	-4.56×10^{-8}	*d*
b_3	3.00×10^{-7}	*c*	b_{134}	-1.06×10^{-8}	*d*
b_4	1.68×10^{-7}	*d*	b_{135}	4.34×10^{-8}	*d*
b_5	-6.31×10^{-7}	*c*	b_{145}	-1.58×10^{-8}	*d*
b_{23}	1.09×10^{-7}	*d*	b_{234}	3.31×10^{-8}	*d*
b_{13}	-4.60×10^{-9}	*d*	b_{235}	-5.04×10^{-9}	*d*
b_{12}	1.91×10^{-7}	*a*	b_{245}	7.67×10^{-8}	*d*
b_{34}	3.52×10^{-7}	*c*	b_{345}	-6.17×10^{-8}	*d*
b_{24}	-1.21×10^{-7}	*d*	b_{1234}	2.33×10^{-7}	*a*
b_{14}	-1.85×10^{-8}	*d*	b_{1235}	1.31×10^{-7}	*d*
b_{25}	4.38×10^{-8}	*d*	b_{1245}	-1.11×10^{-7}	*d*
b_{35}	9.51×10^{-9}	*d*	b_{1345}	8.93×10^{-8}	*d*
b_{15}	2.83×10^{-7}	*b*	b_{2345}	5.95×10^{-8}	*d*
b_{45}	-3.44×10^{-8}	*d*	b_{12345}	-1.28×10^{-7}	*d*

[a] $P > 0.05$ [b] $P > 0.01$ [c] $P > 0.001$ [d] Not significant.

receptor-positive tumors. In vivo PDT efficacy with compound **8** is under investigation.

Experimental Section

Chemistry and Photophysical Studies. Melting points were determined using a Reichert Köfler hot-stage apparatus and are uncorrected. Infrared spectra were recorded with a FTIR Nicolet/Avatar. Routine nuclear magnetic resonance were recorded on a Brucker AM400 spectrometer operating at 400 MHz. Chemical shifts are reported in ppm, relative to the solvent peak, and are given downfield from TMS. Splitting pattern abbreviations are as follows: s = singlet, d = doublet, dd = double doublet, *t* = triplet, td = triplet of doublets, m = multiplet. Electrospray ionization (ESI) mass spectra were recorded on a Surveyor mass spectrometer. Moisture-sensitive reactions were carried out under a dry nitrogen atmosphere in flame-dried glassware. Solvents were distilled before use under nitrogen. Reactions were monitored by thin layer chromatography (TLC) on Merck precoated silica gel 60 F_{254} neutral plates. Silica gel 60 (230−400 mesh) was used for column chromatography. Chemicals were obtained from commercial sources and used without purification, unless stated otherwise. 2,2′-(Ethylenedioxy)-bis-ethylamine was prepared according to ref 57. Methyl 4-formylbenzoate was prepared according to ref 58. Synthesis and purification of folate-containing compounds was performed under reduced light, and these materials should be considered light-sensitive.[59]

Absorption spectra were recorded on a Perkin-Elmer (Lambda 2, Courtaboeuf, France) UV−visible spectrophotometer. Fluorescence spectra were recorded on a Fluorolog-3 spectrofluorimeter *F*222 (Jobin Yvon, Longjumeau, France) equipped with a thermostatted cell compartment (25 °C) using a 450 W xenon lamp. The Φ_F values were determined by the equation: $\Phi_F(\text{sample}) = (F_{\text{sample}}/F_{\text{ref}})(A_{\text{ref}}/A_{\text{sample}})(n_{\text{sample}}{}^2/n_{\text{ref}}{}^2)\Phi_{F(\text{ref})}$, where F, A, and n are the measured fluorescence (area under the emission peak), the absorbance at the excitation wavelength, and the refractive index of the solvent, respectively. Tetraphenylporphyrin (TPP) in toluene was used as reference [$\Phi_{F(\text{ref})} = 0.11$].[60] Determination of singlet oxygen quantum yield $\Phi(^1O_2)$: Excitation occurred with a Xe-arc, the light was separated in a Fluorolog-3 spectrofluorimeter F222, 0.22 μm double monochromator. The detection at 1270 nm was done through a PTI S/N 1565 monochromator, and the emission was monitored by a liquid nitrogen-cooled Ge-detector model (EO-817L, North Coast Scientific Co). The absorbance of the reference solution (Bengal pink in EtOH $\Phi(^1O_2) = 0.68$)[60] and the sample solution (at 515 nm) were set equal (between 0.2 and 0.5) by dilution.

Final compounds **1** and **8** undergoing biological testing were respectively analyzed by HPLC and RP-HPLC using a Shimadzu system. Their purity was found to be above 99%.

5,10,15-tris(3-Methoxyphenyl)-20-(4-methylbenzoate)porphyrin (2). Under a nitrogen flow, a 3-neck flask (2 L) was charged with anhydrous CH_2Cl_2 (1.5 L), freshly distilled pyrrole (1.0 g, 15 mmol), 3-methoxybenzaldehyde (1.53 g, 11.25 mmol), and methyl 4-formylbenzoate (0.62 g, 3.75 mmol). After stirring for 15 min at rt, $BF_3 \cdot OEt_2$ (185 μL) was added. The mixture was further stirred for 2 h at rt. *p*-Chloranil (2.77 g, 11.25 mmol) was then added, and the mixture was refluxed for 2 h. After cooling to rt, the solvent was removed in vacuo. The crude material obtained was purified by gradient column chromatography (CH_2Cl_2/hexanes 1:1 to CH_2Cl_2), yielding **2** (905 mg, 8%) as a purple solid. TLC (CH_2Cl_2): $R_f = 0.59$. ^{1}H NMR ($CDCl_3$): δ 8.95−8.83 (m, 8H, CH β-pyrrole), 8.47 (d, $J = 8.0$ Hz, CH^{Ar}), 8.31 (d, $J = 8.0$ Hz, CH^{Ar}), 7.86−7.80 (m, 6H, CH^{Ar}), 7.67 (dd, $J = J' = 7.6$ Hz, 3H, CH^{Ar}), 4.14 (s, 3H, $COOCH_3$), 4.01 (s, 9H, OCH_3), −2.80 (s, 2H, NH). UV−vis (AcOEt): λ_{max} 415, 512, 548, 588, 645 nm. MS *m*/*z* 763.2 $[M + H]^+$.

5,10,15-tris(3-Methoxyphenyl)-20-(4-carboxyphenyl)porphyrin (3). Compound **2** (0.570 g, 0.74 mmol) and KOH (2.1 g, 0.374 mmol) were suspended in MeOH/THF/pyridine (20:10:1, 24 mL). The reaction mixture was refluxed for 24 h, until TLC showed no ester remaining. After cooling to rt and neutralization with a saturated aqueous solution of citric acid, MeOH and THF were removed in vacuo. The product was extracted with CH_2Cl_2 (2 × 100 mL). The combined organic layers were washed with brine (50 mL) and dried over Na_2SO_4. The crude material obtained was purified by gradient column chromatography (CH_2Cl_2/hexanes 0:1 to 1:0 then acetone), to afford **3** (490 mg, 88%) as a purple solid. TLC (acetone/CH_2Cl_2 2:8): $R_f = 0.73$. IR, ν cm^{-1}: 1707 (C═O). ^{1}H NMR ($CDCl_3$): δ 8.95−8.80 (m, 8H, CH β-pyrrole), 8.54 (d, $J = 7.8$ Hz, 2H, CH^{Ar}), 8.36 (d, $J = 7.8$ Hz, 2H, CH^{Ar}), 7.87−7.75

Table 4. Influence of Animal's Diet (Folate Levels) on **8** Accumulation in KB, HT-29 tumor tissues, and Corresponding Normal Epithelial Tissue (Skin) in Tumor-Bearing Nude Mice[a]

tumor bearing nude mice	diet	tissue type	respective equations	estimated Y value ($\hat{Y}$)	ratio value
RF^+ KB tumor	with folate diet	tumor	$\hat{Y}(\overline{X_1}, \underline{X_2}, \overline{X_3}, \overline{X_4}, \overline{X_5})$	2.42×10^{-6}	1.9
		skin	$\hat{Y}(\underline{X_2}, \underline{X_3}, \underline{X_4}, \underline{X_5})$ __	1.27×10^{-6}	
	with folate-free diet	tumor	$\hat{Y}(\underline{X_1}, \underline{X_2}, \underline{X_3}, X_4, X_5)$	$\mathbf{3.53 \times 10^{-6}}$	**5.0**
		skin	$\hat{Y}(X_2, X_3, \underline{X_4}, \underline{X_5})$ __	$\mathbf{7.12 \times 10^{-7}}$	
RF^- HT-29 tumor	with folate diet	tumor	$\hat{Y}(X_1, \underline{X_2}, \underline{X_3}, X_4, X_5)$	2.66×10^{-6}	2.1
		skin	$\hat{Y}(X_2, \underline{X_3}, \underline{X_4}, \underline{X_5})$ __	1.27×10^{-6}	
	with folate-free diet	tumor	$\hat{Y}(\underline{X_1}, \underline{X_2}, \underline{X_3}, X_4, X_5)$	6.90×10^{-7}	1.0
		skin	$\hat{Y}(X_2, X_3, X_4, X_5)$	7.12×10^{-7}	

[a] Estimation of the tumor-to-normal epithelial tissue ratio based on the multifactor model defined in (3) (see Experimental section).

Table 5. Influence of Animal's Diet (Folate Levels) on **1** Accumulation in KB, HT-29 Tumor Tissues, and in Corresponding Normal Epithelial Tissue (Skin) in Tumor-Bearing Nude Mice[a]

tumor bearing nude mice	diet	tissue type	respective equations	estimated Y value ($\hat{Y}$)	ratio value
RF^+ KB tumor	with folate diet	tumor	$\hat{Y}(\overline{X_1}, \underline{X_2}, \overline{X_3}, \overline{X_4}, \overline{X_5})$	3.73×10^{-6}	2.8
		skin	$\hat{Y}(\underline{X_2}, \underline{X_3}, \underline{X_4}, \underline{X_5})$ __	1.33×10^{-6}	
	with folate-free diet	tumor	$\hat{Y}(\underline{X_1}, \underline{X_2}, \underline{X_3}, X_4, X_5)$	$\mathbf{1.52 \times 10^{-6}}$	2.1
		skin	$\hat{Y}(X_2, X_3, \underline{X_4}, \underline{X_5})$ __	$\mathbf{7.27 \times 10^{-7}}$	
RF^- HT-29 tumor	with folate diet	tumor	$\hat{Y}(X_1, \underline{X_2}, \underline{X_3}, X_4, X_5)$	1.43×10^{-6}	1.1
		skin	$\hat{Y}(X_2, \underline{X_3}, \underline{X_4}, \underline{X_5})$ __	1.33×10^{-6}	
	with folate-free diet	tumor	$\hat{Y}(\underline{X_1}, \underline{X_2}, \underline{X_3}, X_4, X_5)$	2.66×10^{-6}	3.7
		skin	$\hat{Y}(X_2, X_3, X_4, X_5)$	7.27×10^{-7}	

[a] Estimation of the tumor-to-normal epithelial tissue ratio based on the multifactor model defined in (3) (see Experimental Section).

(m, 6H, CH^{Ar}), 7.65 (dd, $J = J' = 8.0$ Hz, 3H, CH^{Ar}), 7.35 (brd, 3H, CH^{Ar}), 3.99 (s, 9H, OCH_3), −2.78 (s, 2H, NH). UV−vis (AcOEt): λ_{max} 415, 512, 546, 589, 645 nm. MS *m/z* 749.3 $[M + H]^+$.

5,10,15-tris(3-Hydroxyphenyl)-20-(4-carboxyphenyl)porphyrin (4). A flask and cooler were dried at 100 °C and cooled under a N_2 flow. Ph_2S_2 (428 mg, 2 mmol) in anhydrous NMP (2 mL) were introduced followed by CaH_2 (230 mg, 5.5 mmol). The reaction mixture was heated at 100 °C for 15 min and then cooled down to rt. In the dark, a solution of porphyrin **3** (490 mg, 0.66 mmol) in NMP (2 mL) was injected, and the mixture was refluxed for 2 h. The resulting reaction mixture was allowed to cool to rt and then poured into 10 mL of a 5 wt % aqueous NaOH solution. The aqueous phase was washed with Et_2O (2 × 5 mL), neutralized with 0.1 N aqueous HCl and extracted with CH_2Cl_2 (3 × 10 mL). The combined CH_2Cl_2 layers were dried over Na_2SO_4. The crude product was purified by gradient flash chromatography (CH_2Cl_2, then acetone, then MeOH/acetone 5:95), yielding **4** (390 mg, 84%) as a dark-purple solid. TLC (acetone): $R_f = 0.46$. IR, ν cm^{-1}: 3206 (OH), 1721 (C═O). ^1H NMR (DMSO-d_6): δ 8.97−8.86 (m, 8H, CH β-pyrrole), 8.41 (d, $J = 7.2$ Hz, 2H, CH^{Ar}), 8.22−8.04 (m, 3H, CH^{Ar}), 7.71−7.56 (m, 6H, CH^{Ar}), 7.31 (brd, 3H, CH^{Ar}), −2.90 (s, 2H, NH). UV−vis (EtOH): λ_{max} 415, 517, 545, 597, 652 nm. MS *m/z* 707.2 $[M + H]^+$.

5,10,15-tris(3-Hydroxyphenyl)-20-(4-carboxyphenyl)chlorin (1). In the absence of light and under N_2, compound **4** (390 mg, 0.55 mmol) and anhydrous K_2CO_3 were added to pyridine (6 mL). Toluene-4-sulfonohydrazide (163 mg, 0.876 mmol) was then added, and the mixture was refluxed for 24 h. Further quantities of toluene-4-sulfonohydrazide (163 mg, 0.876 mmol) were added after 2, 4, 6, and 8 h reaction. After cooling to rt, ethyl acetate (170 mL) and distilled water (100 mL) were added and the reaction mixture was again refluxed for 1 h. After cooling to rt, the organic phase was separated and washed with 2 M HCl (200 mL) and then with water until neutrality. The presence of chlorin and bacteriochlorin was controlled by UV−vis spectroscopy (bands at 651 and 738 nm, respectively). *ortho*-Chloranil was then gradually added to the stirred organic solution at 25 °C until the absorption peak at 738 nm disappeared. The organic phase was then washed with water (200 mL), dried with Na_2SO_4, and concentrated in vacuo. The crude material obtained was purified by gradient column chromatography (CH_2Cl_2/acetone 1:0 to 0:1) to afford **1** as a brown film (360 mg, 66%). TLC (acetone): $R_f = 0.44$. IR, ν cm^{-1}: 3241 (OH), 1719 (C═O). ^1H NMR (DMSO-d_6): δ 8.64 and 8.59 (2d, $J = 4.5$ Hz, 2H, CH β-pyrrole), 8.41−8.02 (m, 10H, CH^{Ar} + CH β-pyrrole), 7.50 (dd, $J = 7.2$ Hz, 3H, CH^{Ar}), 7.30 (d, $J = 7.2$ Hz, 3H, CH^{Ar}), 7.27 (brs, 3H, CH^{Ar}), 7.15 and 7.11 (2dd, $J = 7.2$, $J' = 1.1$ Hz, 3H, CH^{Ar}), 4.21−4.13 (m, 4H, CH_2 β-pyrrole), −1.60 and −1.69 (2s, 2H, NH). UV−vis (EtOH): λ_{max} 417, 517, 542, 597, 650 nm. MS *m/z* 709.2 $[M + H]^+$.

***tert*-Butyl *N*-{2-[2-(2-aminoethoxy)ethoxy] Ethyl Carbamate}-5,10,15-*tris*(3-Hydroxyphenyl)-20-(4-carboxyphenyl)chlorin (6).** In the absence of light and under N_2, chlorin **1** (160 mg, 0.23 mmol) and Boc-protected 2,2′-(ethylenedioxy)-bis-ethylamine **5** (66 mg, 0.27 mmol) were dissolved in anhydrous THF (30 mL). DMAP (28 mg, 0.23 mmol) and EDC (72 mg, 0.37 mmol) were then added, and the mixture was stirred 24 h at rt. The solvent was evaporated in vacuo, and the crude product was purified by gradient flash chromatography (CH_2Cl_2/acetone 1:0 to 0:1) to afford **6** as a brown film (146 mg, 71%). TLC (acetone/CH_2Cl_2 3:7): $R_f = 0.56$. IR, ν cm^{-1}: 1711 (C═O). ^1H NMR (CD_3OD): δ 8.64 and 8.59 (2d, $J =$ 4.5 Hz, CH β-pyrrole), 8.46 (d, $J = 4.5$ Hz, 1H, CH^{Ar}), 8.45−8.39 (m, 3H, CH^{Ar}), 8.29−8.20 (m, 2H, CH^{Ar}), 8.07−7.98 (m, 2H, CH^{Ar}), 7.52−7.05 (m, 12H, CH^{Ar}), 4.17−4.11 (m, 4H, CH_2 β-pyrrole), 4.07 (t, $J = 6.8$ Hz, 2H, CH_2−NHBoc), 3.69−3.11 (m, 10H, OCH_2 + $NHCH_2$), 1.34 (s, 9H, $C(CH_3)_3$). UV−vis (EtOH): λ_{max} 419, 517, 545, 597, 652 nm. MS *m/z* 939.4 $[M + H]^+$.

***N*-{2-[2-(2-Aminoethoxy)ethoxy]ethyl}-5,10,15-tris(3-hydroxyphenyl)-20-(4-carboxyphenyl)chlorin (7).** In the dark under a N_2 atmosphere, compound **6** (146 mg, 0.16 mmol) was treated with TFA/CH_2Cl_2 (1:1, 5 mL) at 0 °C. After being stirred for 2 h, TFA and CH_2Cl_2 were evaporated. The green residue was taken up in CH_2Cl_2 (10 mL), and anhydrous potassium carbonate was added until the color changed from green to red. After filtration, the organic layer was concentrated and the crude product was purified by gradient flash chromatography (CH_2Cl_2/acetone 1:1 to 0:1) to afford **7** as a red film (120 mg, 91%). TLC (acetone): $R_f = 0.24$. IR, ν cm^{-1}: 3284 (NH_2), 1718 (C═O). ^1H NMR (CD_3OD): δ 8.61 and 8.55 (2d, $J = 4.6$ Hz, 2H, CH β-pyrrole), 8.45−8.35 (m, 2H, CH^{Ar}), 8.25−8.12 (m, 3H, CH^{Ar}), 8.07−7.91 (m, 3H, CH^{Ar}), 7.57−7.01 (m, 12H, CH^{Ar}), 4.18−4.02 (m, 4H, CH_2 β-pyrrole), 3.78−3.51 (m, 10H, OCH_2 + $NHCH_2$), 3.09 (t, $J = 6.6$ Hz, 2H, CH_2NH_2), −1.69 (brs, 2H, NH). UV−vis (EtOH): λ_{max} 420, 518, 545, 597, 652. MS *m/z* 838.3 $[M + H]^+$.

{γ-{*N*-{2-[2-(2-Aminoethoxy)ethoxy]ethyl}folic acid}}-5,10,15-tris(3-hydroxyphenyl)-20-(4-carboxyphenyl)chlorin (8). In the dark under a N_2 atmosphere, folic acid (40 mg, 0.1 mmol) and DCC (20 mg, 0.1 mmol) were dissolved in anhydrous DMSO (5 mL) and pyridine (2 mL) and the mixture was stirred for 15 min at rt. Compound **7** (75 mg, 0.09 mmol) was then added and the

reaction mixture was further stirred for 24 h at rt. After filtration, the DMSO solution was slowly poured into vigorously stirred ice-cold Et_2O (100 mL). The dark-red precipitate obtained was collected by filtration and washed with Et_2O (2 × 20 mL) and CH_2Cl_2 (2 × 20 mL) to afford crude **8**. Crude **8** was dissolved in DMSO/H_2O (1/4, 10 mL), and the solution was centrifuged to remove trace insolubles. The supernatant was dialyzed in Spectra/Por tubing (MW cutoff 1000) against saline (50 mM, 2 × 2 L) and water (3 × 2 L) to remove nonreacted folic acid. The dialyzate was lyophilized, and the residue was purified by RP-HPLC on a C_{18} semipreparative column (250 mm × 10 mm I.D., Apollo, Alltech) using a (v/v) water/ methanol gradient, monitored by both absorbance at 415 nm on a SPD-10A UV−visible detector (Shimadzu) and fluorescence on a RF 10AXL fluorescence detector (Shimadzu). Gradient elution conditions were adopted. The eluting solvent was MeOH/H_2O (75:25, v:v) for 15 min followed by 100% methanol for the last 10 min. Room temperature and a flow rate of 4.0 mL/min were maintained throughout the time of purification. A volume of 1 mL of sample in methanol was injected in the column. ^{1}H NMR (DMSO-d_6): δ 11.32 (brs, 2H, folate N^3H and folate N^2H, exchanges with D_2O), 9.81 (brs, 1H, OH), 8.64 (s, 1H, CH^{Ar}), 8.62 and 8.67 (2d, J = 4.6 Hz, 2H, CH β-pyrroleβ), 8.38 and 8.37 (2d, J = 4.6 Hz, 2H, CH β-pyrrole), 8.31−8.14 (m, 6H, CH^{Ar}), 7.61 (d, J = 8.4 Hz, CH^{Ar}), 7.54−7.45 (m, 3H, CH^{Ar}), 7.33−7.28 (m, 3H, CH^{Ar}), 7.10 (d, J = 7.2 Hz, 3H, CH^{Ar}), 6.90 (brs, 1H, NH), 6.63 (d, J = 8.4 Hz, 2H, CH^{Ar}), 4.49−4.40 (m, 4H, CH_2 β-pyrrole), 4.36 (m, 1H, CH^{glu}), 4.17 (brs, 2H, CH_2NHPh, s in D_2O), 3.64−3.18 (m, 12H, CH_2O + CH_2NH), 2.29−2.14 (m, 2H, CH_2^{glu}), 1.94−1.85 (m, 2H, CH_2^{glu}), −1.60 and −1.71 (2s, 2H, NH). UV−vis (EtOH): λ_{max} 283, 417, 517, 542, 596, 650 nm. HRMS (ESI): m/z calcd for $C_{70}H_{63}N_{13}O_{11}$ $[M + H]^+$, 1262.48; found, 1262.4.

Cell Cultures. Cell culture materials were purchased from Costar (Dutscher, Brumath, France), culture media and additives from Life Technologies (Gibco BRL, Cergy-Pontoise, France), except for fetal calf serum, which was obtained from Costar. All other chemicals were purchased from Sigma (Quentin Fallavier, France). KB, human head and neck carcinoma cell line, was obtained from Professor A. Hanauske (Munich University, Germany) as part of the EORTC Preclinical Therapeutic Models Group exchange program and HT-29, human colon cancer cells, was purchased from the American Type Culture Collection. KB and HT-29 cells were grown in 75 cm^2 plastic tissue culture flasks in RPMI 1640 medium supplemented with 9% heat inactivated fetal calf serum, penicillin (100 IU/mL), and streptomycin (100 μg/mL) in a 37 °C, 5% CO_2 atmosphere.

Expression of Folate Receptor type α (FR-α) by Western Blot. The expression of FR-α in KB and HT-29 cells was analyzed by Western blot. HeLa, human cervical cancer cells, was also used to compare the level of FR-α expression with KB cells. A549 are human alveolar basal epithelial cells well-known to be deficient in FR-α expression. They were added as negative control. Hela, A549, KB, and HT-29 monolayer cells were grown in Petri dishes, washed with ice-cold phosphate buffered saline (PBS), and treated with lysis buffer containing 50 mM Tris-HCl, 150 mM NaCl, 2 mM ethylene diamine tetraacetic acid (EDTA), 0.5% Triton X-100 (pH 7.2), and 10% protease cocktail inhibitor (Sigma, Buchs, Switzerland) for 30 min on ice, and further centrifuged at 7000g for 10 min at 4 °C. Total protein concentration was determined using the BCA kit (Pierce, Socochim, Switzerland), according to the manufacturer's instructions. Protein samples (30 μg) were separated on a 8% denaturing polyacrylamide gel without heating or 2-mercaptoethanol treatments prior to loading and followed by electrophoretic transfer to nitrocellulose membrane (Schleicher and Schuell, Dassel, Germany). Membranes were blocked with 5% (w/v) nonfat dry milk in PBS containing 0.05% (v/v) Tween-20 (PBST) for 1 h at room temperature. Membranes were then incubated for 1 h at room temperature with anti-FR antibody (ab3361, abcam, Cambridge, UK), diluted 1:500 in 1% (w/v) nonfat dry milk in PBST. After several washes, the blots were incubated with secondary antimouse antibody linked to horseradish peroxidase (A9044, Sigma, Buchs, Switzerland) and diluted 1:2000 in 1% (w/v) nonfat dry milk in PBST. Bound antibody was detected using the ECL detection system (Amersham Biosciences, Orsay, France) and visualized by autoradiography. Membranes were stained with Ponceau solution (Sigma, Buchs, Switzerland) to check equal loading in each lane.

Animals and Tumors. Female athymic Swiss nude mice (nu/nu) were obtained from Harlan (Gannat, France), and used at 7−9 weeks old and weighted 20−25 g. Animal procedures were performed according to institutional and national guidelines. For all procedures, mice were anesthetized by intraperitoneal injection of 0.01 mL/g of body weight of a solution containing 6 mg/mL ketamine (Panpharma, Fougères, France) and 0.8 μg/mL xylazine (Bayer Pharma, Puteaux, France).

Tumor model xenografted (KB or HT-29) were obtained subcutaneously by injecting a suspension of cells (10^6 cells in 0.1 mL 0.9% NaCl) in either of the hind legs of different mouse (single-tumor mouse model). Quantitative fluorescence measurements of mice with subcutaneous tumors were performed when the tumors reached approximately 200 mm^3 in size. Some of mice used in the reported biodistribution experiments were exclusively fed folate-free rodent diet ad libitum for 2−3 weeks prior to drug administration.

In Vivo Accumulation. When tumors reached the required volume (15 ± 5 days after tumor grafting), **1** and **8** dissolved in polyethylene glycol (PEG) 400−ethanol−water (30/20/50, v/v/v) was injected via the tail vein, and mice were kept in the dark. After a time ranging from 4 to 24 h, mice were anesthetized as previously described. Mice were sacrificed by cervical dislocation. At least three animals were used per time point.

Fluorescence measurements of mice were performed with an optical fiber spectrofluorimeter built in our laboratory. The excitation source used was a laser module (Laser 2000, λ = 410 nm, $\Delta\lambda$ = 3 nm) and an output power of 300 μW. The optical probe was an optical fiber bundle composed of three fibers, one (550 μm core) for excitation light delivery, one (200 μm core) for fluorescence, and one for the backscattered light collection. A long pass filter (Oriel 455FG 03-25) with a 97% transmittance at 500 nm was used on the emission path. The spectrometer used (USB 2000-Ocean Optics) was connected to a computer and a dedicated software. For fluorescence measurements, the distal end of the probe was placed in gentle contact with the tissue area. To evaluate measurement variations, three spectra were performed per site with an accumulation time of 0.5−1 s and then averaged. The three sites were analyzed for each tissue and averaged representing intratissue variations for one animal. Standard errors (SE) were only calculated for intratissue variations. Two or three animals for each condition tested. The fluorescence was first recorded from tumor tissue and consecutively from skin localized on the opposite side of the mouse.

Spectral Analysis. Spectral data sets resulting from spectrofluorimetry analysis of a multicomponent substance are assumed to be a linear combination of the unknown pure component spectra. The identification of the chemical composition of the substance is generally expressed as a source separation problem where the sources correspond to the pure spectra and the mixing coefficients allow estimation of the amount of each component in the substance. The separation algorithm is based on a Bayesian approach coupled to a Markov chain Monte Carlo method, which consists in considering the problem as a decomposition into elementary signals, Gaussian functions in this case.[61] The algorithm was implemented in Matlab (Mathworks Inc.). The relative root-mean-square error between the measured, and the estimated spectra was always lower than 4%. The Gaussian function, which describes the photosensitizer spectrum (located at about 661 nm) was isolated from the estimated model of the complete spectrum. Gaussian function area (Z) was considered in the sequel as a linear function of the in vivo photosensitizer concentration. The fluorescence intensities (Z values) deduced from spectra were corrected to molar extinction coefficient values at 417 nm and to fluorescence quantum yield assessed for each photosensitizer.

Design of Experiments. The purpose of the modeling study was to determine a black-box model describing the mean effects of four

biological factors on the in vivo photosensitizer accumulation in tumors. The output variable noted Y is defined by:

$$Y = \frac{Z}{\varepsilon \cdot \Phi_F} \quad (1)$$

where ε and Φ_F denote the absorption coefficient and the fluorescence quantum yield of the photosensitizer, respectively. The significance of the coefficients was evaluated by the F-test (a, $P > 0.05$; b, $P > 0.001$; c, $P > 0.001$, and ns for not significant).[62] Five two-level biological factors were studied. A list of these factors is presented in Table 2. The full factorial experiment is composed of 32 different trials. Each trial was repeated three times. The coefficient of variation calculated over all the repeated experiments was about 36%.

Multifactor analysis of variance. The description of Y is based on a full factorial model, defined as follows:

$$Y = \hat{Y} + e \quad (2)$$

$$Y = Y_0 + \sum_i b_i \cdot X_i + \sum_{i \neq j} b_{ij} \cdot X_i \cdot X_j + \sum_{i \neq j \neq k} b_{ijk} \cdot X_i \cdot X_j \cdot X_k + \sum_{i \neq j \neq k \neq l} b_{ijkl} \cdot X_i \cdot X_j \cdot X_k \cdot X_l + b_{12345} \cdot X_1 \cdot X_2 \cdot X_3 \cdot X_4 \cdot X_5 \quad (3)$$

with $i,j,k,l \in \{1,2,3,4,5\}$. $\hat{Y}$denotes the estimate of Y, and e is the residual variable. A multifactor analysis of variance based on a least-squares method was performed using the outcomes of the factorial experiment and the R software environment.[62–65] The estimation algorithm is inspired from the one described by Chambers et al.[63]

Estimation of the Mean Effects of the Folate Diet on the in Vivo Selectivity. The selectivity criterion was defined as the tumor-to-skin ratio, i.e., $Y(X_5)/Y(\overline{X_5})$ where the notations X_5, $\overline{X_5}$ denote $X_5 = 1$ and $X_5 = -1$, respectively.

Acknowledgment. J.G. was supported by a grant from the CNRS and la Région Lorraine. This work was supported by the research funds of the French "Ligue Nationale Contre le Cancer, Comités Lorrains". We also gratefully acknowledge Vincent Mazet (Laboratoire des Sciences de l'Image, de l'Informatique et de la Télédétection, Strasbourg, France) for his scientific support in spectrofluorimetry analysis.

Supporting Information Available: RP-HPLC and HRMS analyses of conjugate **8** and in vivo fluorescence spectra. This material is available free of charge via the Internet at http://pubs.acs.org

References

(1) Pandey, R. K.; Zhang, G. *Porphyrin Handbook*; Kadish, K. M., Smith, K. M., Guilard, R., Eds; Academic Press: San Diego, CA, 2000, Vol. 6.
(2) Mac Donald, I. J.; Dougherty, T. J. Basic Principles of Photodynamic Therapy. *J. Porphyrins Phthalocyanines* **2001**, *5*, 105–129.
(3) Weishaupt, K. R.; Gomer, C. J.; Dougherty, T. J. Identification of singlet oxygen as the cytotoxic agent in photo inactivation of a murine tumor. *Cancer Res.* **1976**, *36*, 2326–2329.
(4) Mitchell, J.; Mc Pherson, S.; Degraff, W.; Gamson, J.; Zabell, A.; Russo, A. Oxygen dependence of hematoporphyrin derivative-induced photoinactivation of Chinese hamster cells. *Cancer Res.* **1985**, *45*, 2008–2011.
(5) Castano, A. P.; Liu, Q.; Hamblin, M. R. A green fluorescent protein-expressing murine tumour but not its wild type counterpart is cured by photodynamic therapy. *Br. J. Cancer* **2006**, *94*, 391–397.
(6) Ali, H.; Vautier, J. E. Metal complexes as photo- and radiosensitizers. *Chem. Rev.* **1999**, *99*, 2379–2450.
(7) Nyman, E. S.; Hynninen, P. H. Recent advances in the use of tetrapyrrolic photosensitizers for photodynamic therapy. *J. Photochem. Photobiol. B* **2004**, *73*, 1–28.
(8) Detty, M. R.; Gibson, S. L.; Wagner, S. J. Current clinical and preclinical photosensitizers for use in photodynamic therapy. *J. Med. Chem.* **2004**, *47*, 3897–3915.
(9) Atif, M.; Dyer, P. E.; Paget, T. A.; Snelling, H. V.; Stringer, M. R. Two-photon excitation studies of *m*-THPC photosensitizer and photodynamic activity in an epithelial cell line. *Photodiagn. Photodyn. Ther.* **2007**, *4*, 106–111.
(10) Vrouenraets, M. B.; Visser, G. W.; Snow, G. B.; Van Dongen, G. A. Basic principles, applications in oncology and improved selectivity in photodynamic therapy. *Anticancer Res.* **2003**, *23*, 505–522.
(11) Sharman, W. M.; Allen, C. M.; Van Lier, J. E. Photodynamic therapeutics: basic principles and clinical applications. *Drug Discovery Today* **1999**, *4*, 507–517.
(12) Westerman, P.; Glanzmann, T.; Andrejevic, S.; Braichotte, D. R.; Forrer, M.; Wagnieres, G. A.; Monnier, P.; van den Bergh, H.; Mach, J. P.; Folli, S. Long circulating half-life and high tumor selectivity of the photosensitizer *meta*-tetrahydroxyphenylchlorin conjugated to polyethylene glycol in nude mice grafted with a human colon carcinoma. *Int. J. Cancer* **1998**, *76*, 842–850.
(13) Cramers, P.; Ruevekamp, M.; Oppelaar, H.; Dalesio, O.; Baas, P.; Stewart, F. A. Foscan uptake and tissue distribution in relation to photodynamic efficacy. *Br. J. Cancer* **2003**, *88*, 283–290.
(14) Peng, Q.; Moan, J.; Ma, L. W.; Nesland, J. M. Uptake, localization, and photodynamic effect of *meso*-tetra(hydroxyphenyl)porphine and its corresponding chlorin in normal and tumor tissues of mice bearing mammary carcinoma. *Cancer Res.* **1995**, *55*, 2620–2626.
(15) Schneider, R.; Tirand, L.; Frochot, C.; Vanderesse, R.; Thomas, N.; Gravier, J.; Guillemin, F.; Barberi-Heyob, M. Recent improvements in the use of synthetic peptides for selective photodynamic therapy. *Curr. Med. Chem. Anti-Cancer Agents* **2006**, *6*, 469–488.
(16) Vrouenraets, M. B.; Visser, G. W.; Loup, C.; Meunier, B.; Stigter, M.; Oppelaar, H.; Stewart, F. A.; Snow, G. B.; Van Dongen, V. A. Targeting of a hydrophilic photosensitizer by use of internalizing monoclonal antibodies: A new possibility for use in photodynamic therapy. *Int. J. Cancer* **2000**, *88*, 108–114.
(17) Shadidi, M.; Sioud, M. Selective targeting of cancer cells using synthetic peptides. *Drug. Resist. Updates* **2003**, *6*, 363–371.
(18) Garin-Chesa, P.; Campbell, I.; Saigo, P. E.; Lewis, J. L., Jr.; Old, L. J.; Rettig, W. J. Trophoblast and ovarian cancer antigen LK26. Sensitivity and specificity in immunopathology and molecular identification as a folate-binding protein. *Am. J. Pathol.* **1993**, *142*, 557–567.
(19) Lu, Y. J.; Low, P. S. Folate-mediated delivery of macromolecular anticancer therapeutic agents. *Adv. Drug Delivery Rev.* **2002**, *54*, 675–693.
(20) Leamon, C. P.; Low, P. S. Delivery of macromolecules into living cells: A method that exploits folate receptor endocytosis. *Proc. Natl. Acad. Sci. U.S.A.* **1991**, *88*, 5572–5576.
(21) Kamen, B. A.; Capdevila, A. Receptor-mediated folate accumulation is regulated by the cellular folate content. *Proc. Natl. Acad. Sci. U.S.A.* **1986**, *83*, 5983–5987.
(22) Parker, N.; Turk, M. J.; Westrick, E.; Lewis, J. D.; Low, P. S.; Leamon, C. P. Folate receptor expression in carcinomas and normal tissues determined by a quantitative radioligand binding assay. *Anal. Biochem.* **2005**, *338*, 284–293.
(23) Turek, J. J.; Leamon, C. P.; Low, P. S. Endocytosis of folate−protein conjugate: Ultrastructural localization in KB cells. *J. Cell Sci.* **1993**, *106*, 423–430.
(24) Dixit, V.; Van der Bossche, J.; Sherman, D. M.; Thompson, D. H.; Andres, R. P. Synthesis and grafting of thioctic acid−PEG−folate conjugates onto Au nanoparticles for selective targeting of folate receptor-positive tumor cells. *Bioconjugate Chem.* **2006**, *17*, 603–609.
(25) Bharali, D. J.; Lucey, D. W.; Jayakumar, H.; Pudavar, H. E.; Prasad, P. N. Folate−receptor-mediated delivery of InP quantum dots for bioimaging using confocal and two-photon microscopy. *J. Am. Chem. Soc.* **2005**, *127*, 11364–11371.
(26) Wang, C.-H.; Hsiue, G. H. Polymer−DNA hybrid nanoparticles based on folate−polyethyleneimine-*block*-poly(L-lactide). *Bioconjugate Chem.* **2005**, *16*, 391–396.
(27) Soppimath, K. S.; Liu, L.-H.; Seow, W. Y.; Liu, S.-Q.; Powell, R.; Chan, P.; Yang, Y. Y. Multifunctional core/shell nanoparticles self-assembled from pH-induced thermosensitive polymers for targeted intracellular anticancer drug delivery. *Adv. Funct. Mater.* **2007**, *17*, 355–362.
(28) Bae, Y.; Jang, W.-D.; Nishiyama, N.; Fukushima, S.; Kataoke, K. Multifunctional polymeric micelles with folate-mediated cancer cell targeting and pH-triggered drug releasing properties for active intracellular drug delivery. *Mol. BioSyst.* **2005**, *1*, 242–250.
(29) Zheng, G.; Chen, J.; Li, H.; Glickson, J. D. Rerouting lipoprotein nanoparticles to selected alternate receptors for the targeted delivery of cancer diagnostic and therapeutic agents. *Proc. Natl. Acad. Sci. U.S.A.* **2005**, *102*, 17757–17762.
(30) Okarvi, S. M.; Jammaz, I. A. Preparation and in vitro and in vivo evaluation of technetium-^{99}m-labeled folate and methotrexate conjugates as tumor imaging agents. *Cancer Biother. Radiopharm.* **2006**, *21*, 49–60.

(31) Salmaso, S.; Semenzato, A.; Caliceti, P.; Hoebeke, J.; Sonvico, F.; Dubernet, C.; Couvreur, P. Specific antitumor targetable β-cyclodextrin-poly(ethyleneglycol)-folic acid drug delivery bioconjugate. *Bioconjugate Chem.* **2004**, *15*, 997–1004.

(32) Leamon, C. P.; Reddy, J. A.; Vlahov, I. R.; Vetzel, M.; Parker, N.; Nicoson, J. S.; Xu, L.-C.; Westrick, E. Synthesis and biological evaluation of EC72: A new folate-targeted chemotherapeutic. *Bioconjugate Chem.* **2005**, *16*, 803–811.

(33) Nayak, S.; Lee, H.; Chmielewski, J.; Lyon, L. A. Folate-mediated cell targeting and cytotoxicity using thermoresponsive microgels. *J. Am. Chem. Soc.* **2004**, *126*, 10258–10259.

(34) Myc, A.; Majoros, I. J.; Thomas, T. P.; Baker, J. R., Jr. Dendrimer-based targeted delivery of an apoptotic sensor in cancer cells. *Biomacromolecules* **2007**, *8*, 13–18.

(35) Sabharanjak, S.; Mayor, S. Folate receptor endocytosis and trafficking. *Adv. Drug Delivery Rev.* **2004**, *56*, 1099–1109.

(36) Leamon, C. P.; Reddy, J. A. Folate-targeted chemotherapy. *Adv. Drug Delivery Rev.* **2004**, *56*, 1127–1141.

(37) Schneider, R.; Schmitt, F.; Frochot, C.; Fort, Y.; Lourette, N.; Guillemin, F.; Muller, J. F.; Barberi-Heyob, M. Design, Synthesis and biological evaluation of folic acid targeted tetraphenylporphyrin as novel photosensitizers for selective photodynamic therapy. *Bioorg. Med. Chem.* **2005**, *13*, 2799–2808.

(38) Stefflova, K.; Li, H.; Chen, J.; Zheng, G. Peptide-based pharmacomodulation of a cancer-targeted optical imaging and photodynamic therapy agent. *Bioconjugate Chem.* **2007**, *18*, 379–388.

(39) Chakraborti, A. K.; Nayak, M. K.; Sharma, L. Diphenyl disulfide and sodium in NMP as an efficient protocol for in situ generation of thiophenate anion: Selective deprotection of aryl alkyl ethers and aryl/aryl esters under nonhydrolytic conditions. *J. Org. Chem.* **2002**, *67*, 1776–1780.

(40) Gavande, N. S.; Kundu, S.; Badqujar, N. S.; Kaw, G.; Chakraborti, A. K. Ph_2S_2-CaH_2 in *N*-methyl-2-pyrrolidinone as an efficient protocol for chemoselective cleavage of aryl alkyl ethers. *Tetrahedron* **2006**, *62*, 4201–4204.

(41) Laville, I.; Pigaglio, S.; Blais, J.-C.; Loock, B.; Maillard, P.; Grierson, D. S.; Blais, J. A study of the stability of tri(glucosyloxyphenyl)chlorin, a sensitizer for photodynamic therapy in human colon tumoral cells: a liquid chromatography and MALDI-TOF mass spectrometry analysis. *Bioorg. Med. Chem.* **2004**, *12*, 3673–3682.

(42) Wang, S.; Low, P. S. Folate-mediated targeting of antineoplastic drugs, imaging agents, and nucleic acids to cancer cells. *J. Controlled Release* **1998**, *53*, 39–48.

(43) Wang, S.; Lee, R. J.; Mathias, C. J.; Green, M. A.; Low, P. S. Synthesis, purification, and tumor cell uptake of ^{67}Ga-desferoxamine-folate, a potential radiopharmaceutical for tumor imaging. *Bioconjugate Chem.* **1996**, *7*, 56–62.

(44) Mantovani, L. T.; Miotti, S.; Ménard, S.; Canevari, S.; Raspagliesi, F.; Bottini, C.; Bottero, F.; Colnaghi, M. I. Folate binding protein distribution in normal tissues and biological fluids from ovarian carcinoma patients as detected by the monoclonal antibodies MOv18 and MOv19. *Eur. J. Cancer* **1994**, *30*, 363–369.

(45) Ross, J. F.; Chaudhuri, P. K.; Ratnam, M. Differiential regulation of folate receptor isoforms in normal and malignant tissues in vivo and established cell lines: Physiologic and clinical implications. *Cancer* **1994**, *73*, 2432–2443.

(46) Bourdon, O.; Laville, I.; Carrez, D.; Croizy, A.; Fedel, Ph.; Kasselouri, A.; Prognon, P.; Legrand, P.; Blais, J. Biodistribution of *meta*-tetra(hydroxyphenyl)chlorin incorporated into surface-modified nanocapsules in tumor-bearing mice. *Photochem. Photobiol. Sci* **2002**, *1*, 709–714.

(47) Wagnières, G. A.; Star, W. M.; Wilson, B. C. In vivo fluorescence spectrometry and imaging for oncological applications. *Photochem. Photobiol.* **1998**, *68*, 603–632.

(48) Mathias, C. J.; Wang, S.; Lee, R. J.; Waters, D. J.; Turek, J. J.; Low, P. S.; Green, M. A. Tumor-selective radiopharmaceutical targeting via receptor mediated endocytosis of gallium-67-deferoxamine-folate. *J. Nucl. Med.* **1996**, *37*, 1003–1008.

(49) Paulos, C. M.; Reddy, J. A.; Leamon, C. P.; Turk, M. J.; Low, P. S. Ligand binding and kinetics of folate receptor recycling in vivo: Impact on receptor-mediated drug delivery. *Mol. Pharmacol.* **2004**, *66*, 1406–1414.

(50) Ma, L.; Steindal, A. E.; Juzeniene, A.; Iani, V.; Moan, J. The effect of folic acid on porphyrin synthesis in tumors and normal skin of mice treated with 5-aminolevulinic-acid or methyl 5-aminolevulinate. *Photochem. Photobiol. Sci.* **2006**, *5*, 755–759.

(51) Bryce, R.; Hettiaratchy, S.; Clarke, J.; Taubel, J.; Besa, C.; Smith, R. Burns after photodynamic therapy. *Br. J. Med* **2000**, *320*, 1731–1732.

(52) Morlet, L.; Vonarx-Coinsmann, V.; Lenz, P.; Foultier, M. -T.; Xavier de Brito, L.; Stewart, C.; Patrice, T. Correlation between *meta*(tetrahydroxyphenyl)chlorin (*m*-THPC) biodistribution and photodynamic effect in mice. *J. Photochem. Photobiol., B* **1995**, *28*, 25–32.

(53) Whelpton, R.; Michael-Titus, A. T.; Basra, S. S.; Grahn, M. Distribution of Temoporfin, a new photosensitizer for the photodynamic therapy of cancer in a murine tumor model. *Photochem. Photobiol.* **1995**, *61*, 397–401.

(54) Whelpton, R.; Michael-Titus, A. T.; Jamdar, R. P.; Abdillahi, K.; Grahn, M. Distribution and excretion of radiolabeled Temoporfin in a murine tumor model. *Photochem. Photobiol.* **1996**, *63*, 885–891.

(55) Glanzmann, T.; Forrer, M.; Andrejevic Blant, S.; Woodtli, A.; Grosjean, P.; Braichotte, D.; Van der Berg, H.; Monnier, P.; Wagnières, G. Pharmacokinetics and pharmacodynamics of tetra(*m*-hydroxyphenyl)chlorin in the hamster cheek pouch tumor model: Comparison with clinical measurements. *J. Photochem. Photobiol., B* **2000**, *57*, 22–32.

(56) Ronn, A. M.; Batti, J.; Lee, C. J.; Yoo, D.; Siegel, M. E.; Nouri, M.; Lofgren, M. A.; Steinberg, B. M. Comparative biodistribution of *meta*-tetra(hydroxyphenyl)chlorin in multiple species: Clinical implications for photodynamic therapy. *Lasers Surg. Med.* **1997**, *20*, 437–442.

(57) Trester-Zedlitz, M.; Kamada, K.; Burley, S. K.; Fenyol, D.; Chait, B. T.; Muir, T. W. A Modular cross-linking approach for exploring protein interactions. *J. Am. Chem. Soc.* **2003**, *125*, 2416–2425.

(58) Gimenez, R.; Oriol, L.; Pinol, M.; Serrano, J. L.; Vinuales, A. I.; Fisher, T.; Stumpe, J. Synthesis and properties of 2-phenylbenzoxazole-based luminophores for in situ photopolymerized liquid-crystal films. *Helv. Chim. Acta* **2006**, *89*, 304–319.

(59) Thomas, A. H.; Suarez, G.; Cabrerizo, F. M.; Martino, R.; Capparelli, A. L. Study of the photolysis of folic acid and 6-formylpterin in acid aqueous solution. *J. Photochem. Photobiol., A* **2000**, *135*, 147–154.

(60) Figueiredo, T.; Johnstone, R.; Santana Sorensen, A.; Burget, D.; Jacques, P. Determination of fluorescence yields, singlet lifetimes, and singlet oxygen yields of water-insoluble porphyrins and metalloporphyrins in organic solvents and in aqueous media. *Photochem. Photobiol.* **1999**, *69*, 517–528.

(61) Mazet, V. Development of methods for spectroscopic signal processing: baseline and spectral peaks estimation. Ph.D. Thesis, Nancy University, December2005.

(62) Box, G. E. P.; Hunter, W. G.; Hunter J. S. *Statistics for Experimenters. An Introduction to Design, Data Analysis, and Model Building*; Wiley Series in Probability and Mathematical Statistics; Wiley & Sons: New York, 1978.

(63) Chambers, J. M.; Freeny, A.; Heiberger, R. M. Analysis of variance; designed experiments. In *Statistical Models in S*; Chambers, J. M., Hastie, T. J., Eds.; Wadsworth & Brooks/Cole: Pacific Grove, CA, 1992; Chapter 5.

(64) Box, G. E. P.; Hunter, W. G.; Hunter J. S. *Statistics for Experimenters. An Introduction to Design, Data Analysis, and Model Building*; Wiley Series in Probability and Mathematical Statistics; Wiley & Sons: New York, 1978.

(65) R Development Core Team. *R: A Language and Environment for Statistical Computing*; R Foundation for Statistical Computing: Vienna, Austria, 2005; ISBN 3-900051-07-0, http://www.R-project.org

JM800125A